第 35 卷第 10 期
2019 年 10 月

无 机 化 学 学 报
CHINESE JOURNAL OF INORGANIC CHEMISTRY

Vol.35 No.10
1791-1804

多卤素取代的 salamo 型锰(Ⅱ)配合物：合成、晶体结构、Hirshfeld 分析及荧光性质

王 岚 魏治利 于 盟 潘迎旗 张 阳 董文魁*

(兰州交通大学化学与生物工程学院，兰州 730070)

摘要：在有机溶剂中，通过卤素取代的 salamo 型双肟配体 H_2L^1(4,4′,6,6′-tetrachloro-2,2′-(ethylenediyldioxybis(nitrilomethylidyne))diphenol)，H_2L^2(5-nitro-4′,6′-dichloro-2,2′-(ethylenedioxybis(azomethine))diphenol)和四水合乙酸锰(Ⅱ)反应，合成了 2 个锰(Ⅱ)配合物 $[Mn(L^1)(H_2O)_2]$ (**1**)和$[Mn(L^2)(H_2O)_2]\cdot 0.37H_2O$ (**2**)，并通过元素分析、红外光谱、紫外-可见吸收光谱、单晶 X 射线衍射、荧光光谱和 Hirshfeld 表面分析对 2 个锰(Ⅱ)配合物进行了表征。X 射线晶体学结果表明 2 个配合物中的锰(Ⅱ)原子都是六配位的，其中 salamo 型配体的 N_2O_2 占据平面位置，2 个配位水分子占据轴向位置，形成了扭曲的八面体几何构型。由于存在较丰富的氢键相互作用，在配合物 **1** 和 **2** 中分别形成了无限的一维和二维超分子结构。

关键词：salamo 型配体；配合物；合成；荧光性质；Hirshfeld 表面分析

中图分类号：O614.71+1　　**文献标识码**：A　　**文章编号**：1001-4861(2019)10-1791-14

DOI：10.11862/CJIC.2019.212

Multihalogen-Substituted Salamo-Type Mn(Ⅱ) Complexes: Syntheses, Crystal Structures, Hirshfeld Analyses and Fluorescence Properties

WANG Lan　WEI Zhi-Li　YU Meng　PAN Ying-Qi　ZHANG Yang　DONG Wen-Kui*

(*School of Chemical and Biological Engineering, Lanzhou Jiaotong University, Lanzhou* 730070, *China*)

Abstract: Two manganese(Ⅱ) complexes $[Mn(L^1)(H_2O)_2]$ (**1**) and $[Mn(L^2)(H_2O)_2]\cdot 0.37H_2O$ (**2**) were synthesized by the reactions of halogen-substituted salamo-type bisoxime ligands H_2L^1, H_2L^2 with manganese (Ⅱ) acetate tetrahydrate in organic solvents, and the two complexes were characterized by the means of elemental analyses, FT-IR, UV-visible absorption spectra, single-crystal X-ray diffractions, fluorescence spectra and Hirshfeld surfaces analyses. X-ray crystallography results indicated that the manganese(Ⅱ) ions in the two complexes are all six-coordinated, in which the N_2O_2 of the salamo-type ligand occupied the planar position, and two coordinated water molecules occupied the axial positions, forming distorted octahedral coordination geometries. Due to abundant hydrogen bonding interactions, infinite 1D and 2D supramolecular structures are formed in complexes **1** and **2**, respectively. CCDC: 1813346, **1**; 1816807, **2**.

Keywords: samalo-type ligand; complex; synthesis; fluorescence property; Hirshfeld surface analysis

0 Introduction

As is generally known, salen-type ligands (R^1-CH=N-$(CH_2)_2$-N=CH-R^2) and their derivatives are a class of important N_2O_2 chelating ligands[1-3], their metal complexes have been extensively investigated in modern coordination chemistry for the past several decades[4-7], because they not only show a variety of

收稿日期：2019-01-15。收修改稿日期：2019-08-06。

国家自然科学基金(No.21761018)资助项目。

*通信联系人。E-mail：dongwk@126.com；会员登记号：02M87091161。

properties in catalytic and optical properties[8-13], but also have some advantages in the fields of antibacterial activities[14-21], electrochemical conducts[22-24], supramolecular buildings[25-32], ions recognitions[33-38] and so on. Recently, new researches have been expanded in the use of salamo-type ligands (R^1-CH=N-O-$(CH_2)_n$-O-N=CH-R^2)[39-43], and their complexes have been applied in a very wide and diversified subjects such as supramolecular architectures[44-45] and luminescence properties[46-49]. As derivatives of salen-type compounds, salamo-type compounds are more significant, because the electronic and steric effects of the ligands on salamo-metal-assisted catalysis may be controlled by the introduction of proper substituents into the benzene rings. Furthermore, it is important to introduce suitable functional groups into the organic moieties of the ligands in order to improve the properties of these metal complexes[50-51]. Now, the synthesis of structurally-specific, superior properties of salamo-type metal complexes, and study of their applications have become an important chemical field and potential areas.

Based on previous works, we have designed and synthesized two multihalogen-substituted salamo-type manganese(Ⅱ) complexes by the coordination reactions of salamo-type bisoxime ligands H_2L^1, H_2L^2 with manganese(Ⅱ) acetate tetrahydrate, respectively. To the best of our knowledge, the aforementioned manganese (Ⅱ) salamo-type complexes haven′t been reported[52-54]. Here, elemental analyses, FT-IR, UV-visible absorption spectra, single-crystal X-ray diffractions, fluorescence spectra and Hirshfeld surfaces of the two manganese (Ⅱ) complexes were investigated in detail to study their structural features and spectral characteristics.

1 Experimental

1.1 Materials and physical measurements

2-Hydroxy-3,5-dichlorobenzaldehyde and 2-hydroxy-5-nitrobenzaldehyde (99%) were purchased from Alfa Aesar and used directly without purification. All other solvents and chemicals were analytical grade and obtained from Tianjin Chemical Reagent Factory. Elemental analysis data of C, H and N were performed on a GmbH VarioEL V3.00 automatic elemental analysis instrument. Elemental analysis for manganese(Ⅱ) was detected with an IRIS ER/S-WP-1 ICP atomic emission spectrometer. Melting points were measured with a microscopic melting point apparatus made by Beijing Taike Instrument Limited Company and were uncorrected. Fourier transform IR spectra were recorded with a VERTEX70 FT-IR spectrophotometer, with samples prepared as KBr (500~4 000 cm^{-1}) and CsI (100~500 cm^{-1}) pellets. UV-visible absorption spectra were collected on a Shimadzu UV-3900 spectrophotometer. Fluorescent spectra were recorded on F-7000 spectrophotometer. Single crystal X-ray structure determinations were made by a SuperNova and Bruker D8 Venture diffractometers, respectively. Hirshfeld surfaces analyses and two-dimensional fingerprint plots of complexes **1** and **2** were calculated using Crystal Explorer program.

1.2 Synthesis of the ligands H_2L^1 and H_2L^2

The major reaction steps, containing the synthesis of 4,4′,6,6′-tetrachloro-2,2′-(ethylenediyldioxybis(nitrilomethylidyne))diphenol (H_2L^1) and 5-nitro-4′,6′-dichloro-2,2′-(ethylenedioxybis(azomethine))diphenol (H_2L^2) are given in Scheme 1.

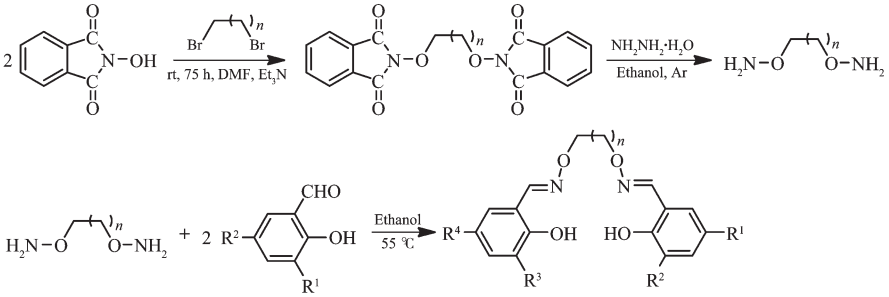

H_2L^1: n=1, R^1=R^2=R^3=R^4=Cl; H_2L^2: n=1, R^1=NO_2, R^2=H, R^3=R^4=Cl

Scheme 1 Syntheses routes to H_2L^1 and H_2L^2

1,2-Bis(aminooxy)ethane was prepared in accordance with the previously literatures[55-56]. Yield: 56.8%. Anal. Calcd. for $C_2H_8N_2O_2$(%): C, 26.08; H, 8.76; N, 30.42. Found(%): C, 25.97; H, 8.70; N, 30.49.

1.2.1　Synthesis of H_2L^1

The salamo-type bisoxime ligand (H_2L^1) was synthesized according to our previous work[54,57]. Fig.1 shows the high resolution mass spectrum of ligand H_2L^1. In the high resolution mass spectrum, a strong peak appeared at m/z=437.030 9, which is consistent with the relative molecular mass determined by the elemental analysis. ^{1}H NMR (500 MHz, DMSO-d_6): δ 4.48 (s, 4H, -CH_2), 7.53 (t, J=2.6 Hz, 2H, -ArH), 7.61 (t, J=2.6 Hz, 2H, -ArH), 8.47 (d, J=2.0 Hz, 2H, -N=CH), 10.38 (s, 2H, -OH). Yield: 72.8%. m.p. 204~205 ℃. Anal. Calcd. for $C_{16}H_{12}Cl_4N_2O_4$(%): C, 43.87; H, 2.76; N, 6.39. Found(%): C, 43.95; H, 2.68; N, 6.28.

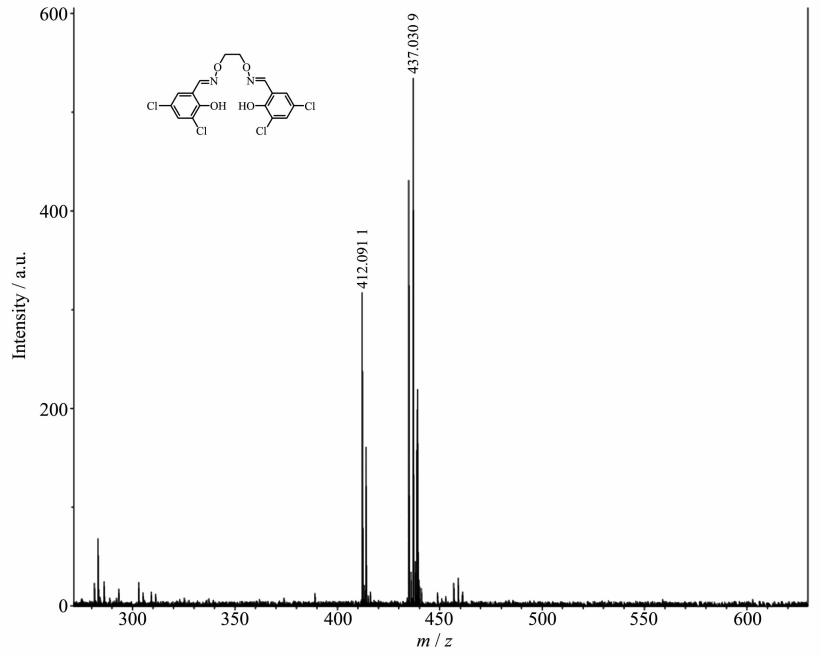

Fig.1　High resolution mass spectrum of H_2L^1

1.2.2　Synthesis of H_2L^2

A solution of 2-hydroxy-3,5-dichlorobenzaldehyde (382.02 mg, 2.0 mmol) in ethanol (100 mL) was added dropwise to a solution of 1,2-bis (aminooxy)ethane (368.4 mg, 4.0 mmol) in ethanol (40 mL), then the mixture was subjected to heating at 55 ℃ for 6 h. The solution was concentrated in vacuum and the residue was purified by column chromatography (SiO_2, chloroform/ethyl acetate, 25:1, V/V) to afford 2-(*O*-(1-ethyloxyamide))oxime-4,6-dichlorophenol. Yield: 65.6%, m.p. 92~93 ℃. Anal. Calcd. for $C_9H_{10}Cl_2N_2O_3$(%): C, 40.78; H, 3.80; N, 10.57. Found(%): C, 40.92; H, 3.69; N, 10.63.

2-Hydroxy-5-nitrobenzaldehyde (334.24 mg, 2.0 mmol) was dissolved in the ethanol solution (15 mL) and added to a stirred colorless ethanol solution (20 mL) of the above-obtained 2-(*O*-(1-ethyloxyamide)) oxime-4,6-dichlorophenol (530.18 mg, 2 mmol). The mixture was heated and stirred at 55 ℃ about 6 h before being allowed to cool to room temperature. Then the suspension solution was filtered and washed with ethanol/hexane (1:4, V/V). After dried under vacuum, the resulting white solid of H_2L^2 was collected. The high resolution mass spectrum and nuclear magnetic resonance spectrum of the ligand H_2L^2 are shown in Fig.2 and 3, respectively. A strong peak appeared at m/z=412.096 0 in the high resolution mass spectrum, which is consistent with the relative molecular mass determined by the elemental analysis. ^{1}H NMR (500 MHz, DMSO-d_6): δ 4.48 (s, 4H, -CH_2), 7.07 (dd, J=9.0, 3.0 Hz, 1H, -ArH), 7.53 (d, J=2.5 Hz, 1H, -ArH), 7.59 (d, J=2.5 Hz, 1H, -ArH), 8.15 (dd, J=9.0, 3.0 Hz, 1H,

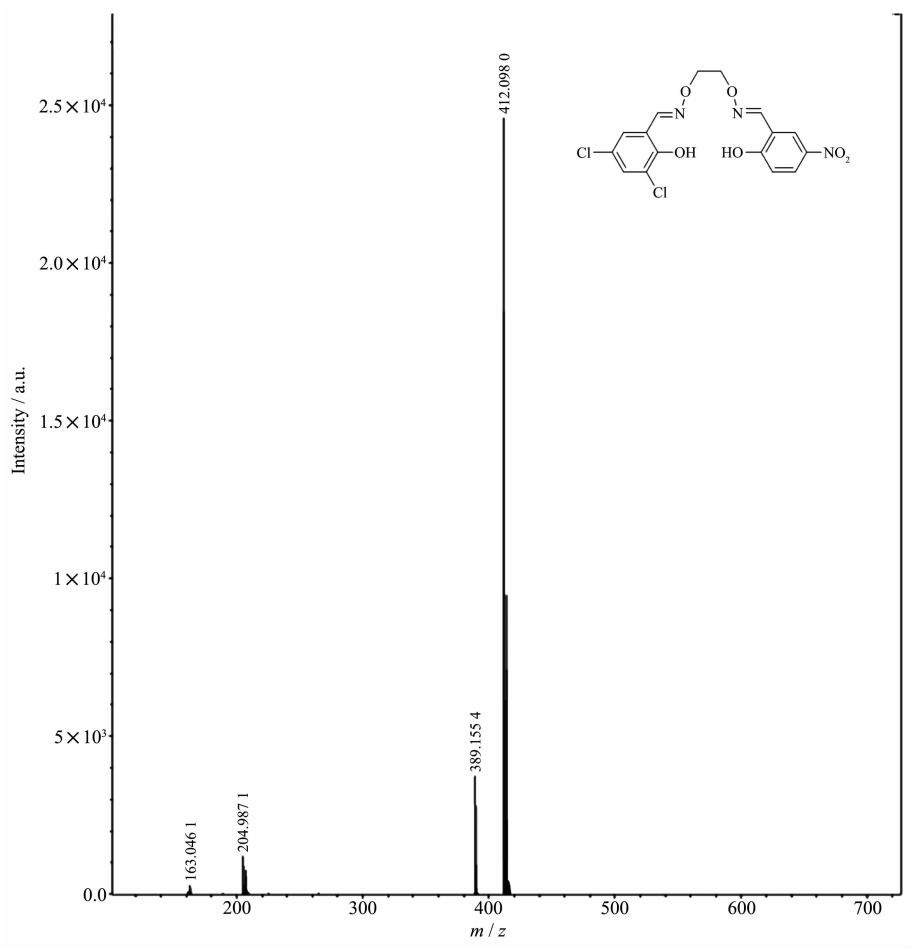

Fig.2 High resolution mass spectrum of H_2L^2

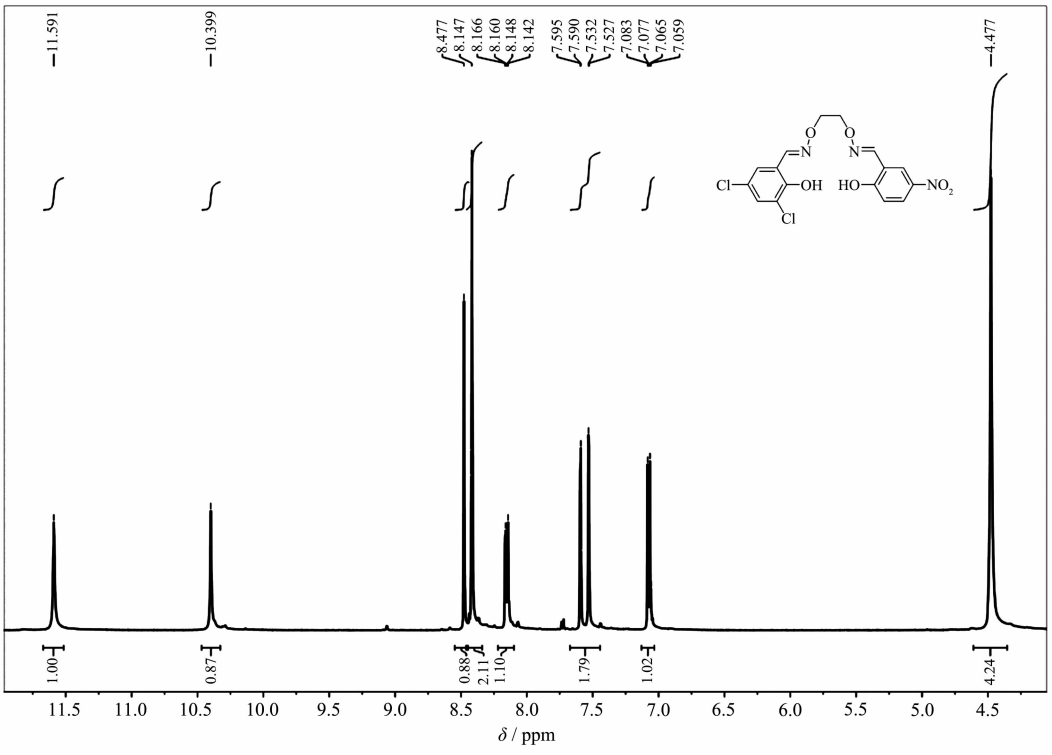

Fig.3 ^{1}H NMR spectrum of H_2L^2

-ArH), 8.42 (s, 2H, -N=CH), 8.48 (s, 1H, -ArH), 10.40 (s, 1H, -OH), 11.59 (s, 1H, -OH). Yield: 68%. m.p. 174 ~175 ℃. Anal. Calcd. for $C_{16}H_{13}Cl_2N_3O_6$(%): C 46.40; H 3.16; N 10.14. Found(%): C 46.59; H 3.05; N 10.03.

1.3 Syntheses of complexes 1 and 2

1.3.1 Synthesis of complex **1**

A solution of manganese(Ⅱ) acetate tetrahydrate (2.45 mg, 0.014 mmol) in mixed solvent of methanol (2.0 mL) and ethanol (3.0 mL) was added dropwise to a chloroform solution (3.0 mL) of H_2L^1 (2.19 mg, 0.005 mmol) at room temperature. The color of the mixing solution turned brown immediately. After the mixture was stirred for 1 h, the mixture was filtered. The resulting filtrate was left undisturbed for about several days to form clear light brown block-like crystals suitable for X-ray crystallographic analysis. Yield: 45.7%. Anal. Calcd. for $C_{16}H_{14}Cl_4MnN_2O_6$(%): C, 36.46; H, 2.68; N, 5.32; Mn, 10.42. Found(%): C, 36.74; H, 2.52; N, 5.19; Mn, 10.59.

1.3.2 Synthesis of complex **2**

A mixed solution of methanol (2.0 mL) and ethanol (4.0 mL) of manganese(Ⅱ) acetate tetrahydrate (3.72 mg, 0.015 mmol) was added to a chloroform solution (3.0 mL) of H_2L^2 (2.07 mg, 0.005 mmol) at room temperature. After the mixture was stirred for 2 h, the mixture was fltered off. The resulting fltrate was left undisturbed for about one week to form block-like crystals suitable for X-ray crystallographic analysis. Yield: 40.5%. Anal. Calcd. for $C_{16}H_{15.73}Cl_2MnN_3O_{8.37}$(%): C, 37.70; H, 3.11; N, 8.24; Mn, 10.78. Found (%): C, 37.75; H, 3.22; N, 8.06; Mn, 10.64.

1.4 Crystal structure determinations of complexes 1 and 2

The single crystal of complex **1** with approximated dimensions of 0.21 mm×0.15 mm×0.12 mm was placed on a SuperNova diffractometer. The diffraction data were collected using a graphite monochromated Mo $K\alpha$ radiation source (λ=0.071 073 nm) at 293(2) K. While the X-ray diffraction data of complex 2 with approximated dimensions of 0.26 mm×0.22 mm×0.20 mm was placed on a Bruker D8 Venture diffractometer. The diffraction data were collected using a graphite monochromated Mo $K\alpha$ radiation source (λ=0.071 073 nm) at 291(2) K. In addition, multi-scan absorption corrections were applied. The crystal structures were solved using direct methods and refined anisotropically by the full-matrix least-squares techniques based on F^2 with SHELXL-2014/7[58] and SHELXL-2018 programs[58], respectively. The positions for hydrogen atoms were fixed on geometrically idealized positions and refined via a riding model. The non-hydrogen atoms were refined anisotropically with displacement parameters. Selected data of collection parameters and structure refinement of complexes **1** and **2** are summarized in Table 1.

CCDC: 1813346, **1**; 1816807, **2**.

Table 1　Crystal data and refinement parameter for complexes 1 and 2

Complex	1	2
Formula	$C_{16}H_{14}Cl_4MnN_2O_6$	$C_{16}H_{15.73}Cl_2MnN_3O_{8.37}$
Formula weight	527.03	509.81
Crystal system	Monoclinic	Triclinic
Space group	*C*2/*c*	$P\bar{1}$
a / nm	1.728 35(17)	0.764 9(2)
b / nm	1.515 65(17)	1.159 4(2)
c / nm	0.776 92(6)	1.427 0(2)
α / (°)		110.121(6)
β / (°)	97.161(9)	100.257(9)
γ / (°)		102.123 4(19)
V / nm^3	2.019 3(3)	1.117 7(4)
Z	4	2

Continued Table 1

D_c / (g·cm^{-3})	1.734	1.515
μ / mm^{-1}	1.220	0.877
F(000)	1 060	517
θ range / (°)	3.314~26.993	3.329~25.996
Index ranges	$-21 \leqslant h \leqslant 21, -19 \leqslant k \leqslant 18, -9 \leqslant l \leqslant 5$	$-7 \leqslant h \leqslant 9, -14 \leqslant k \leqslant 14, -17 \leqslant l \leqslant 17$
Reflection collected	4 100	8 032
Independent reflection	2 172	4 234
R_{int}	0.016 2	0.028 6
Data, restraint, parameter	2 172, 1, 127	4 234, 3, 291
GOF	1.099	0.995
Final R_1, wR_2 indices [$I>2\sigma(I)$]	0.043 8, 0.125 4	0.054 9, 0.134 1
R_1, wR_2 indices (all data)	0.057 6, 0.136 8	0.075 4, 0.140 5
Largest differences peak and hole / (e·nm^{-3})	990, −488	425, −330

2 Results and discussion

2.1 FT-IR spectra

Infrared spectroscopy of complexes **1** and **2** are measured at various bands within the region of 4 000~100 cm^{-1} and major infrared bands are delineated in Table 2.

It can be seen from the IR spectra that the C=N stretching vibration band of H_2L^1 exhibited a characteristic absorption at 1 609 cm^{-1}, and that of complex **1** appeared at 1 607 cm^{-1}. A typical Ar=O vibration band in H_2L^1 emerged at 1 217 cm^{-1}, and that of complex **1** was at approximately 1 209 cm^{-1}. The changes in the spectrum of complex **1** show that M-N/O interactions were formed in the IR spectrum upon complexation. In addition, the appearance of new medium intensity bands for complex **1** at approximately 463 and 511 cm^{-1} were attributed to M-N and M-O stretching vibration bands. The infrared spectrum of complex **1** showed the expected absorption bands at *ca.* 3 395, 1 637 and 557 cm^{-1} which could be assigned to the coordinated water molecules, indicating the presence of coordinated water molecules[59]. The facts mentioned above are in accordance with the results of crystal X-ray diffractions.

A typical C=N stretching band of the free ligand H_2L^2 appeared at 1 614 cm^{-1}, and that of complex **2** appeared at 1 602 cm^{-1}. The Ar-O vibration band in H_2L^2 emerged at 1 315 cm^{-1}, and that of complex **2** was at approximately 1 285 cm^{-1}. The shift of Ar-O stretching frequencies could be evidence of the Mn-O bond formation between the Mn(Ⅱ) ion and oxygen atoms of phenolic groups. In the far-IR spectrum of complex **2**, the M-O and M-N stretching frequencies were also obtained[60]. The bands at *ca.* 507 and 474 cm^{-1} could be attributed to M-N and M-O vibration bands. The changes in the spectra of complex **2** show that H_2L^2 coordinates with Mn(Ⅱ) ions[61].

Table 2 Main infrared data of H_2L^1, H_2L^2 and their complexes 1 and 2

cm^{-1}

Compound	Ar-O	C=N	M-N	M-O	C=C
H_2L^1	1 217	1 609	—	—	1 462, 1 575, 1 595
1	1 209	1 607	463	511	1 486, 1 579, 1 597
H_2L^2	1 315	1 614			1 475, 1 572, 1 594
2	1 285	1 602	507	474	1 492, 1 578, 1 598

2.2 UV-Vis absorption spectra

UV-Vis spectra of the free ligands in 25 μmol·L^{-1} ethanol solution and their corresponding complexes **1** and **2** in 1.0 mmol·L^{-1} ethanol solution at 298 K were measured within a range of 220~550 nm (Fig.4 and 5).

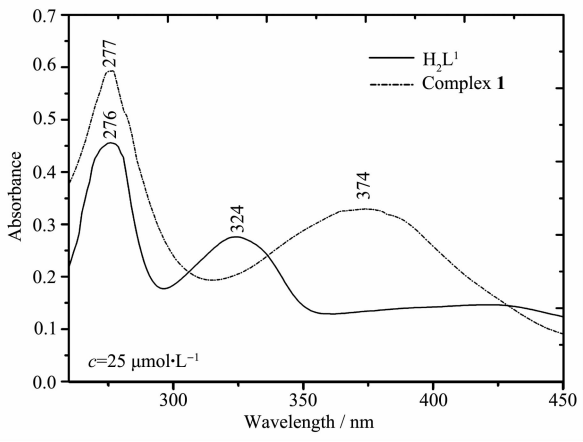

Fig.4　UV-Vis absorption spectra of H_2L^1 and complex **1** in ethanol solution

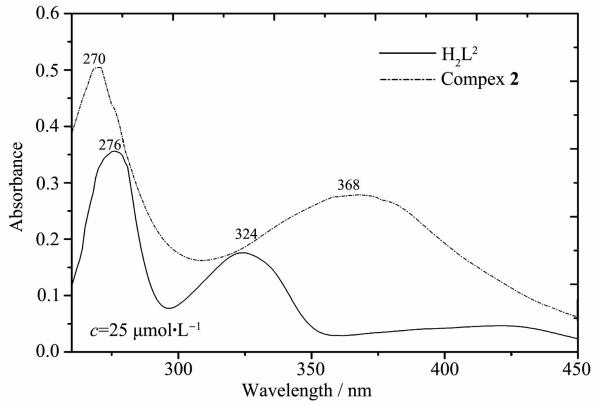

Fig.5　UV-Vis absorption spectra of H_2L^2 and complex **2** in ethanol solution

Obviously, the absorption peaks of ligand H_2L^1 are different from those of complex **1**. The UV-Vis spectrum of H_2L^1 had two relatively intense absorption peaks at ca. 276 and 324 nm. The absorption band at 276 nm could be assigned to the π-π* transition for the benzene rings; and the second peak at 324 nm could be assigned to the n-π* transition for the C=N group. In contrast to H_2L^1, the absorption peaks were bathochromically shifted[62] (Fig.4). These phenomena are owing to the reaction of H_2L^1 with the Mn(Ⅱ) ions.

The absorption spectrum of ligand H_2L^2 shown in Fig.5 included two relatively intense peaks centered at *ca.* 276 and 324 nm, which could be assigned to the π-π* transition for the benzene rings and the n-π* transition for the C=N group. But in complex **2**, the absorption peak at 276 nm showed a hypsochromic shift to 270 nm, and the disappearance of the absorption peak of the ligand at 324 nm might be caused by coordination of the two N atoms of C=N groups with the Mn(Ⅱ) ion. For complex **2**, a new absorption peak appeared at 368 nm due to the transfer of electrons from the ligand to the Mn(Ⅱ) ion.

2.3　Crystal structures of complexes 1 and 2

2.3.1　Crystal structure of complex **1**

X-ray diffraction analysis demonstrated that complex **1** possesses a symmetric mononuclear structure and crystallizes in the monoclinic system with *C*2/*c* space group. Complex **1** is built up by one $C_{16}H_{14}Cl_4MnN_2O_6$ molecule, which contains one Mn(Ⅱ) ion, one completely deprotonated ligand $(L^1)^{2-}$ and two coordinated water molecules. The molecular structure with atomic labeling of complex **1** is depicted in Fig.6. Selected bond lengths and angles of complex **1** are listed in Table 3.

The coordination sphere of the hexa-coordinated Mn(Ⅱ) ion is completed by two phenolic oxygen atoms (Mn1-O2 0.211 97(19) nm and Mn1-O2#1 0.211 98(19) nm) and two nitrogen atoms (Mn1-N1 0.229 3(3) nm and Mn1-N1#1 0.229 3(3) nm) coming from the completely deprotonated unit $(L^1)^{2-}$ and two

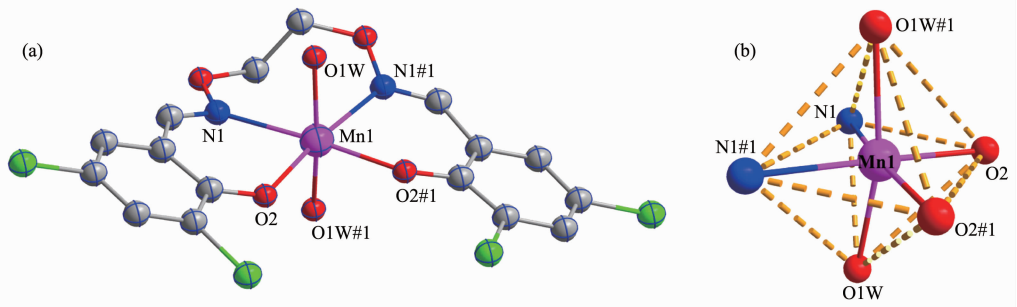

Symmetry codes: #1: 2–*x*, *y*, 1/2–*z*; Hydrogen atoms are omitted for clarity

Fig.6　(a) Molecular structure of complex **1**; (b) Coordination polyhedron for Mn(Ⅱ) ion

Table 3 Selected bond lengths (nm) and angles (°) for complexes 1 and 2

1					
Mn1-O2	0.211 97(19)	Mn1-O1W	0.216 3(2)	Mn1-N1	0.229 3(3)
Mn1-O2#1	0.211 98(19)				
O2-Mn1-O2	93.69(11)	O2-Mn1-O1W	94.44(8)	O1W-Mn1-O1W	167.23(12)
O2-Mn1-N1	80.00(9)	O2-Mn1-O1W#1	94.28(8)	O1W-Mn1-N1	84.88(9)
O2-Mn1-N1#1	173.57(9)	N1-Mn1-N1	106.33(13)	O1W-Mn1-N1#1	87.47(9)
2					
Mn1-O4	0.205 6(3)	Mn1-O1	0.207 7(2)	Mn1-O1W	0.219 9(2)
Mn1-N1	0.221 9(3)	Mn1-N2	0.229 7(3)	Mn1-O2W	0.220 1(2)
O4-Mn1-O1	91.83(10)	O4-Mn1-O1W	83.72(11)	O1-Mn1-O1W	98.09(9)
O4-Mn1-O2W	101.12(11)	O1-Mn1-O2W	85.57(9)	O1W-Mn1-O2W	173.88(9)
O4-Mn1-N1	171.40(11)	O1-Mn1-N1	82.98(9)	O1W-Mn1-N1	90.20(9)
O2W-Mn1-N1	85.37(10)	O4-Mn1-N2	82.46(10)	O1-Mn1-N2	173.75(9)
O1W-Mn1-N2	83.85(9)	O2W-Mn1-N2	93.02(10)	N1-Mn1-N2	102.99(9)

Symmetry codes: #1: 2–*x*, *y*, 1/2–*z* for **1**.

oxygen atoms (Mn1-O1W, 0.216 3(2) nm and Mn1-O1W#1, 0.216 3(2) nm) of the coordinated water molecules. Therefore, the Mn(Ⅱ) ion forms a slightly distorted octahedral geometry. The distances of the Mn(Ⅱ) ion and the phenolic oxygen atoms (O2 and O2#1) of the fully deprotonated $(L^{l})^{2-}$ unit are clearly shorter than those of the nitrogen atoms (N1 and N1#1) from the $(L^{l})^{2-}$ unit (Fig.6). There are one intramolecular hydrogen bond (C8#1–H8B⋯O1W#1), three intermolecular hydrogen bonds (O1W#2–H1A⋯O2#2, O1W#2–H1A⋯Cl1#2, O1W#3–H1B⋯O2#3) in complex **1**, finally forming a 1D supramolecular structure (Fig.7 and 8).

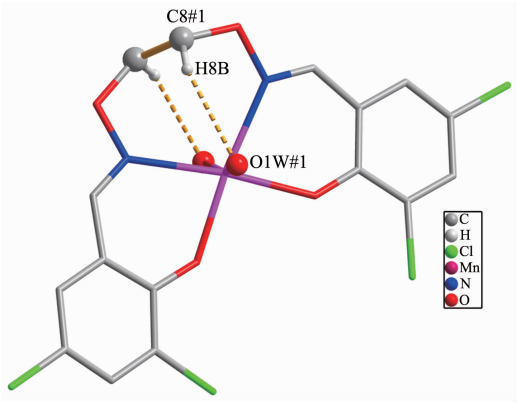

Symmetry codes: #1: 2–*x*, *y*, 1/2–*z*

Fig.7 View of intramolecular hydrogen bonding interactions of complex **1**

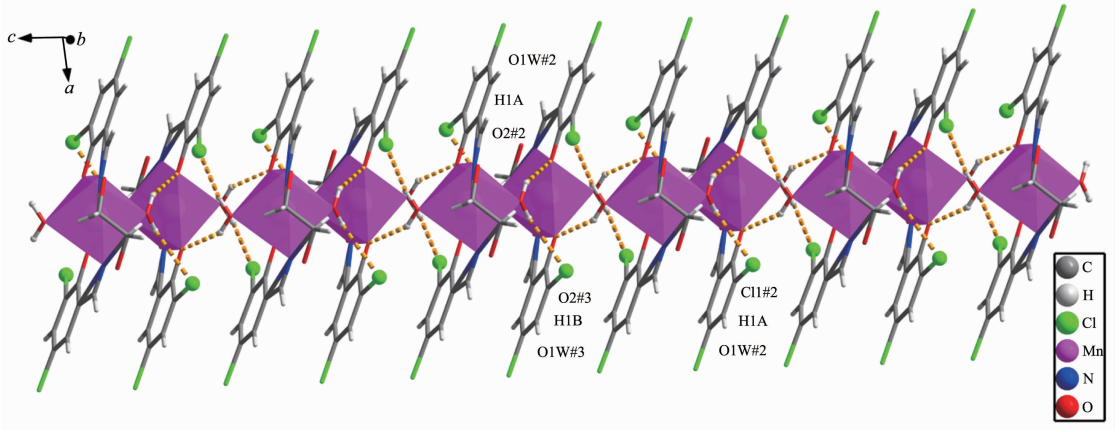

Symmetry codes: #2: 2–*x*, 1–*y*, –*z*; #3: *x*, 1–*y*, –1/2+*z*

Fig.8 View of 1D supramolecular architecture of complex **1** formed by hydrogen bonding interactions

2.3.2　Crystal structure of complex **2**

X-ray crystallographic analysis reveals that complex **2** belongs to triclinic crystal system with space group $P\bar{1}$, and has a symmetric mononuclear structure. Fig.9(a) and (b) showed the molecular structure and the octahedral unit of complex **2**. Selected bond lengths and angles are provided in Table 4.

Single crystal X-ray diffraction analysis showed that the crystal structure of complex **2** was similar to that of complex **1**, forming a 1:1 ($(L^2)^{2-}$ and Mn(Ⅱ)) mononuclear structure. Complex **2** contained one Mn(Ⅱ) ion, one full deprotonated $(L^2)^{2-}$ unit and two coordinated water molecules. The hexa-coordinated Mn(Ⅱ) ion (Mn1) is located in the *cis*-N_2O_2 coordination cavity (Mn1-O1, 0.207 7(2) nm, Mn1-O4, 0.205 6(3) nm, Mn1-N1 0.221 9(3) nm and Mn1-N2 0.229 7(3) nm) of the completely deprotonated $(L^2)^{2-}$ unit, and two oxygen atoms (Mn1-O1W, 0.219 9(2) nm and Mn1-O2W 0.220 1(2) nm) of the coordinated H_2O molecules occupied together the axial positions. All of the six oxygen atoms coordinate to the Mn (Ⅱ) ion (Mn1) constituting an octahedral geometry, as shown in Fig.9 (b). Six intramolecular hydrogen bonds (O1W–H1WA⋯N2, O1W–H1WB⋯O4, O2W–H2WA⋯N1, O2W–H2WB⋯O1, C8–H8A⋯N2 and C9–H9A⋯N1) and four intermolecular hydrogen bonding interactions (O1W#1 –H1WB ⋯ O1#1, O2W#1 –H2WB ⋯ O4#1, C3 –H3#2 ⋯ O3#2 and C14#3 –H14 ⋯ O6#3) are observed and shown in Fig.10. With the help of

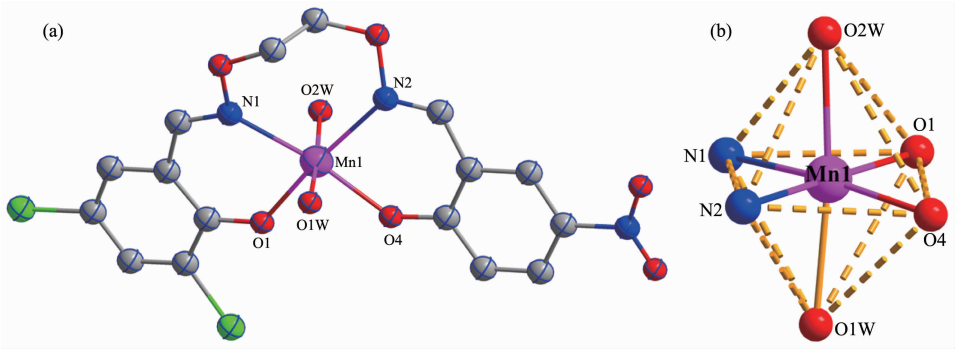

Hydrogen atoms are omitted for clarity

Fig.9　(a) Molecular structure of complex **2**; (b) Coordination polyhedron for Mn(Ⅱ) ion

Table 4　Hydrogen bonding parameters of complexes 1 and 2

D–H⋯A	*d*(D-H) / nm	*d*(H⋯A) / nm	*d*(D⋯A) / nm	∠DHA / (°)
C8#1–H8B⋯O1W#1	0.097	0.252	0.337 9(4)	148
O1W#2–H1A⋯O2#2	0.089	0.210	0.290 9(3)	151.7
O1W#2–H1A⋯Cl1#2	0.089	0.278	0.338 4(2)	127
O1W#3–H1B⋯O2#3	0.088	0.192	0.272 1(3)	149.5
O1W–H1WA⋯N2	0.089	0.251	0.300 5(4)	116
O1W–H1WB⋯O4	0.089	0.240	0.284 1(4)	111
O2W–H2WA⋯N1	0.089	0.251	0.299 6(4)	115
O2W–H2WB⋯O1	0.089	0.246	0.290 7(4)	111
C8–H8A⋯N2	0.097	0.249	0.287 9(5)	104
C9–H9A⋯N1	0.097	0.245	0.286 7(5)	106
O1W#1–H1WB⋯O1#1	0.089	0.213	0.283 1(3)	136
O2W#1–H2WB⋯O4#1	0.089	0.220	0.286 4(4)	131
C3–H3#2⋯O3#2	0.093	0.258	0.346 0(5)	158
C14#3–H14⋯O6#3	0.093	0.252	0.321 1(5)	131

Symmetry codes: #1: 2–*x*, *y*, 1/2–*z*; #2: 2–*x*, 1–*y*, –*z*; #3: *x*, 1–*y*, –1/2+*z* for **1**; #1: 1–*x*, 2–*y*, 1–*z*; #2: *x*, 1+*y*, *z*; #3: 1–*x*, 2–*y*, 2–*z* for **2**.

hydrogen bond interactions in complex **2**, the adjacent complex **2** molecule units are linked together forming an infinite 2D supramolecular network, which is shown in Fig.11.

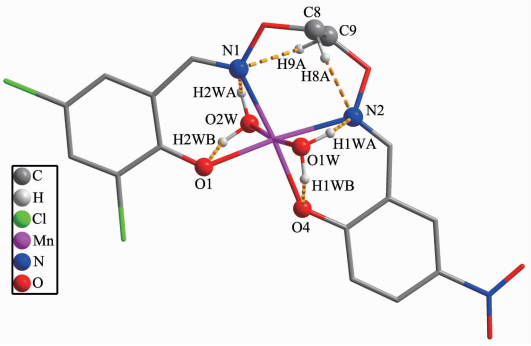

Fig.10 View of intramolecular hydrogen bonding interactions of complex **2**

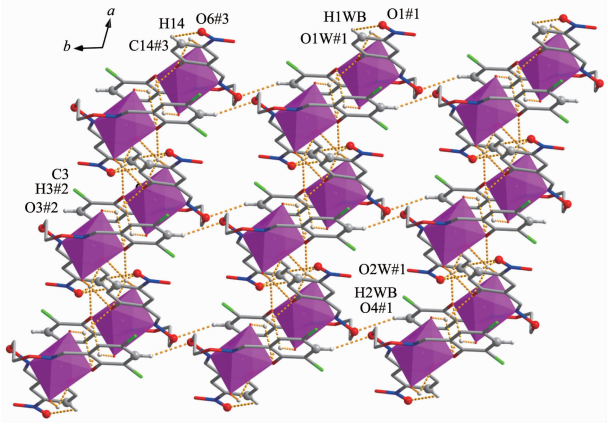

Symmetry codes: #1: 1−*x*, 2−*y*, 1−*z*; #2: *x*, 1+*y*, *z*; #3: 1−*x*, 2−*y*, 2−*z*

Fig.11 View of 2D supramolecular architecture of complex **2** formed by hydrogen bonding interactions

2.4 Hirshfeld surfaces analyses

The Hirshfeld surfaces of the free ligands and their complexes **1** and **2** were analyzed using Crystal Explorer program. The surface analyses of H_2L^1, H_2L^2 and complexes **1** and **2** have been mapped with d_{norm} (standard high resolution), curvedness and shape index (Fig.12)[63]. When mapped with the function of d_{norm}, the surface of H_2L produces several spherical red depressions, indicating the main presence of type C–H ··· O interactions, and other visible depressions correspond to H ··· H and C ··· H interactions. For complexes **1** and **2**, more intense red depressions can be seen on the Hirshfeld surfaces which marks the O ···H/H···O interactions persisting. The 2D fingerprint plots are used to explain the atom pair contacts of the crystal, which can quantify the intermolecular interactions. Meantime, it could be decomposed to highlight contributions from different interactions. The 2D fingerprint plot of H···H, C···H/H···C and O···H/H ··· O interactions in the complexes are depicted in Fig.13.

In complex **1**, the proportions of C···H/H···C, O ··· H/H ··· O, H ··· H and Cl ··· H interactions cover 4.1%, 16.5%, 17.8% and 39.7% of the Hirshfeld surfaces, respectively, while the proportions of C···H/H···C, O···H/H···O, H···H and Cl···H interactions in complex **2** cover 1.7%, 19.1%, 24.4% and 6.6%, respectively. Because of the existence of hydrogen bonds, complexes **1** and **2** can be more stable[64].

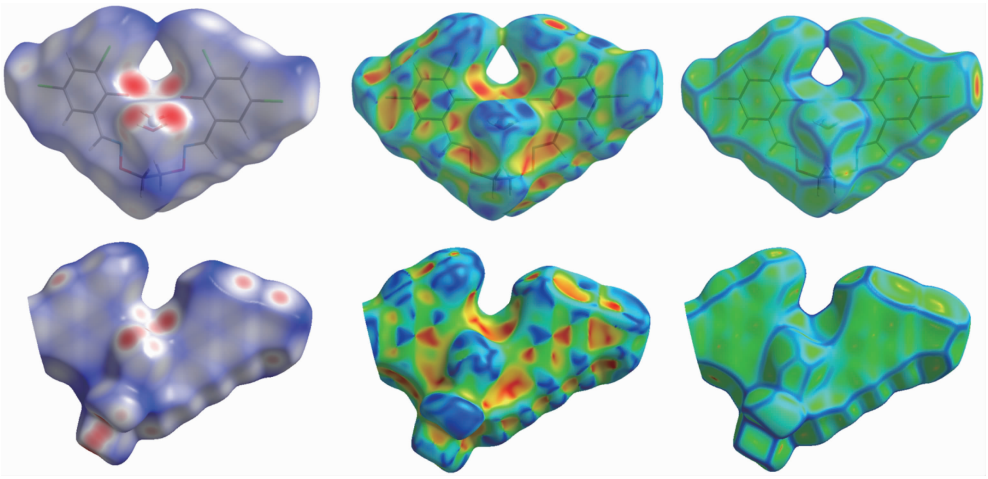

Fig.12 Hirshfeld surfaces of complexes **1** and **2** mapped with d_{norm}, shape index and curvedness

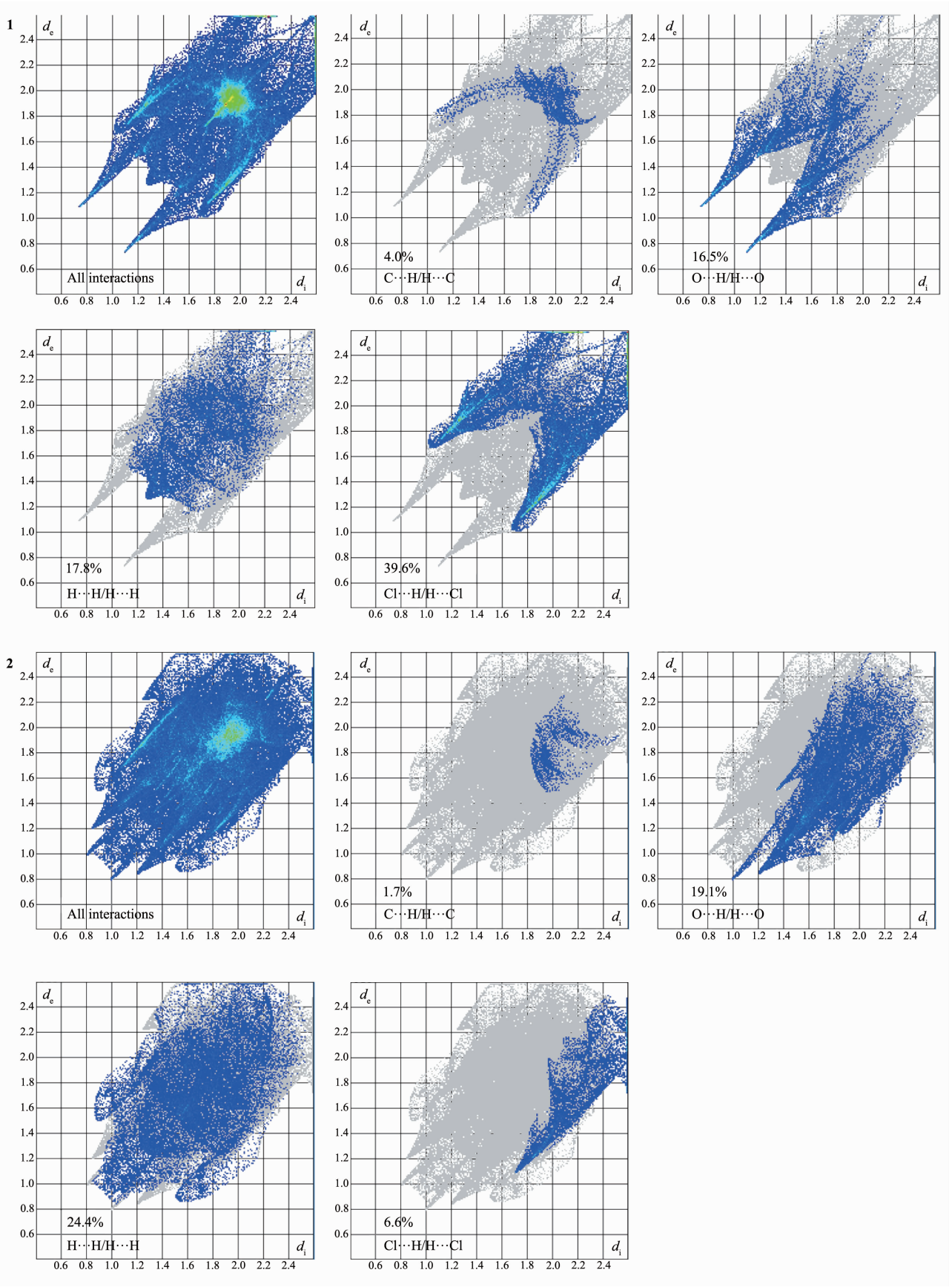

Fig.13　Two dimensional fingerprint plots of complexes **1** and **2** with major decomposition plots

2.5 Fluorescence properties

The fluorescence behaviors of H_2L^1, H_2L^2 and their corresponding complexes **1** and **2** were measured in ethanol solution (25 μmol·L^{-1}) at room temperature within wavelength range of 350~600 nm and displayed in Fig.14~15.

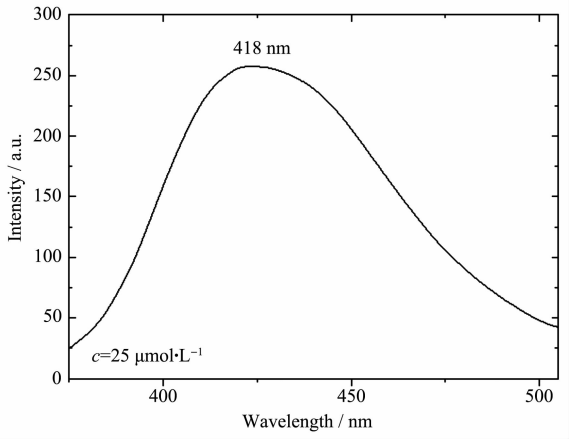

Fig.14 Emission spectra of H_2L^1 and complex **1** in ethanol solution

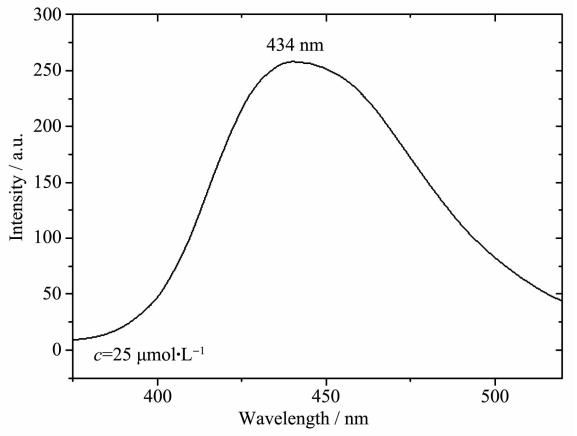

Fig.15 Emission spectra of H_2L^2 and complex **2** in ethanol solution

The spectrum of H_2L^1 is non-fluorescent upon excitation at 370 nm in ethanol solution. However, complex **1** exhibited an intense fluorescence intensity (Fig.14) at 418 nm upon excitation at 370 nm, because of the photoinduced electron transfer mechanism. In complex **1**, the Mn(Ⅱ) ion is coordinated with the lone pair electrons of C =N and phenol oxygen atoms of benzene rings, which enhances the planar steel of the molecules, resulting in enhancement of fluorescence[65].

The spectrum of H_2L^2 is also non-fluorescent upon excitation at 375 nm. But complex **2** exhibited an intense emission peak at *ca.* 434 nm upon excitation at 375 nm (Fig.15), which can be attributed to the photoinduced electron transfer mechanism. As same as complex **1**, the Mn(Ⅱ) ion in complex **2** is coordinated with the N atoms of the C=N group and phenol oxygen atoms of benzene rings, leading to the increased coplanarity of molecule and enhanced fluorescence.

3 Conclusions

In conclusion, we have designed and synthesized two Mn(Ⅱ) complexes with two salamo-type ligands H_2L^1 and H_2L^2, and characterized them by physico-chemical methods and single-crystal X-ray diffractions. X-ray crystal structures revealed that the structural features of complexes **1** and **2** are very similar, and the water molecules participate in the coordination. In the IR spectra of complexes **1** and **2**, the M-O and M-N vibrational absorption bands were observed. The UV-Vis spectra clearly indicate that the ligand $(L^1)^{2-}$ or $(L^2)^{2-}$ units of complexes **1** or **2** are coordinated with the Mn(Ⅱ) ions. The fluorescent results of complexes **1** and **2** showed relatively strong emission peaks compared to the corresponding free ligands. The Hirshfeld surfaces and 2D fingerprint plots could explain the atom pair contacts of the crystal, which could quantify the intermolecular interactions.

Acknowledgements: This work was supported by the National Natural Science Foundation of China (Grant No. 21761018) and the Program for Excellent Team of Scientific Research in Lanzhou Jiaotong University (Grant No.201706), which are gratefully acknowledged.

References:

[1] Liu P P, Wang C Y, Zhang M, et al. *Polyhedron*, **2017**,**129**: 133-140

[2] Song X Q, Liu P P, Liu Y A, et al. *Dalton Trans.*, **2016**,**45**: 8154-8163

[3] Subramaniam P, Anbarasan S, Devi S S, et al. *Polyhedron*, **2016**,**119**:14-22

[4] Akine S, Miyashita M, Piaob S, et al. *Inorg. Chem. Front.*, **2014**,**1**:53-57

[5] Dong X Y, Zhao Q, Kang Q P, et al. *Crystals*, **2018**,**8**:230
[6] Zhang L W, Li X Y, Kang Q P, et al. *Crystals*, **2018**,**8**:173
[7] Li X Y, Kang Q P, Liu L Z. *Crystals*, **2018**,**8**:43
[8] Peng Y D, Li X Y, Kang Q P, et al. *Crystals*, **2018**,**8**:1079
[9] Peng Y D, Wang F, Gao L, et al. *J. Chin. Chem. Soc.*, **2018**, **65**:893-899
[10]Li X Y, Chen L, Gao L, et al. *RSC Adv.*, **2017**,**7**:35905-35916
[11]Xu L, Li N, Zhao L. *Z. Kristallogr.*: *New Cryst. Struct.*, **2016**, **231**:967-968
[12]Li L H, Dong W K, Zhang Y, et al. *Appl. Organomet. Chem.*, **2017**,e3818
[13]Chin T K, Endud S, Jamil S, et al. *Catal. Lett.*, **2013**,**143**: 282-288
[14]Gao L, Liu C, Wang F, et al. *Crystals*, **2018**,**8**:77
[15]Wu H L, Bai Y H, Zhang Y H, et al. *Z. Anorg. Allg. Chem.*, **2014**,**640**:2062-2071
[16]Wu H L, Pan G L, Wang H, et al. *J. Photochem. Photobiol. B*, **2014**,**135**:33-43
[17]Wu H L, Pan G L, Bai Y C, et al. *J. Chem. Res.*, **2014**,**38**: 211-217
[18]Wu H L, Bai Y C, Zhang Y H, et al. *J. Coord. Chem.*, **2014**, **67**:3054-3066
[19]Wang F, Xu Y L, Aderinto S O, et al. *J. Photochem. Photobiol. A*, **2017**,**332**:273-282
[20]Wu H L, Wang H, Wang X L, et al. *New J. Chem.*, **2014**, **38**:1052-1061
[21]Wu H L, Pan G L, Bai Y C, et al. *Res. Chem. Intermed.*, **2015**,**41**:3375-3388
[22]Hao J, Li X Y, Wang L, et al. *Spectrochim. Acta Part A*, **2018**,**204**:388-402
[23]Wang L, Hao J, Zhai L X, et al. *Crystals*, **2017**,**7**:277
[24]Ömer S, Ümmühan Ö Ö, Nurgul S, et al. *Tetrahedron*, **2016**, **72**:5843-5852
[25]Li J, Zhang H J, Chang J, et al. *Crystals*, **2018**,**8**:176
[26]Chai L Q, Zhang K Y, Tang L J, et al. *Polyhedron*, **2017**, **130**:100-107
[27]Dong X Y, Li X Y, Liu L Z, et al. *RSC Adv.*, **2017**,**7**:48394-48403
[28]Jia H R, Chang J, Zhang H J, et al. *Crystals*, **2018**,**8**:272
[29]Chen L, Dong W K, Zhang H, et al. *Cryst. Growth Des.*, **2017**,**17**:3636-3648
[30]Zhang L W, Liu L Z, Wang F, et al. *Molecules*, **2018**,**23**: 1141
[31]Dong X Y, Zhao Q, Wei Z L, et al. *Molecules*, **2018**,**23**: 1006
[32]Chai L Q, Tang L J, Chen L C, et al. *Polyhedron*, **2017**,**122**: 228-240
[33]Dong W K, Li X L, Wang L, et al. *Sens. Actuators B*, **2016**, **229**:370-378
[34]Wang B J, Dong W K, Zhang Y, et al. *Sens. Actuators B*, **2017**,**247**:254-264
[35]Wang F, Gao L, Zhao Q, et al. *Spectrochim. Acta Part A*, **2018**,**190**:111-115
[36]Dong Y J, Li X L, Zhang Y, et al. *Supramol. Chem.*, **2017**,**29**: 518-527
[37]Hao J, Li X Y, Zhang Y, et al. *Materials*, **2018**,**11**:523
[38]Dong W K, Akogun S F, Zhang Y, et al. *Sens. Actuators B*, **2017**,**238**:723-734
[39]Dong W K, Ma J C, Zhu L C, et al. *Cryst. Growth Des.*, **2016**,**16**:6903-6914
[40]Wang L, Li X Y, Zhao Q, et al. *RSC Adv.*, **2017**,**7**:48730-48737
[41]Dong W K, Li G, Wang Z K, et al. *Spectrochim. Acta Part A*, **2014**,**133**:340-347
[42]Hao J, Li L H, Zhang J T, et al. *Polyhedron*, **2017**,**134**:1-10
[43]Zhang H, Dong W K, Zhang Y, et al. *Polyhedron*, **2017**,**133**: 279-293
[44]Ma J C, Dong X Y, Dong W K, et al. *J. Coord. Chem.*, **2016**, **69**:149-159
[45]Hao J, Liu L Z, Dong W K, et al. *J. Coord. Chem.*, **2017**,**70**: 1936-1952
[46]YANG Yu-Hua(杨玉华), HAO Jing(郝静), DONG Yin-Juan(董银娟), et al. *Chinese. J. Inorg. Chem.*(无机化学学报), **2017**,**33**:1280-1292
[47]Akine S, Taniguchi T, Saiki T, et al. *J. Am. Chem. Soc.*, **2005**,**127**:540-541
[48]Zhao Q, Wei Z L, Kang Q P, et al. *Spectrochim. Acta Part A*, **2018**,**203**:472
[49]Dong W K, Zheng S S, Zhang J T, et al. *Spectrochim. Acta Part A*, **2017**,**184**:141-150
[50]ZHANG Hong-Jia(张宏佳), CHANG Jian(常健), JIA Hao-Ran(贾浩然), et al. *Chinese J. Inorg. Chem.*(无机化学学报), **2018**,**34**:2261-2270
[51]CHANG Jian(常健), ZHANG Hong-Jia(张宏佳), JIA Hao-Ran(贾浩然), et al. *Chinese J. Inorg. Chem.*(无机化学学报), **2018**,**34**:2097-2107
[52]Dong W K, Sun Y X, Zhao C Y, et al. *Polyhedron*, **2010**,**29**: 2087-2097
[53]Dong X Y, Wang L, Yang Y H, et al. *Asian J. Chem.*, **2013**, **8**:4289-4292
[54]Dong W K, Zhao C Y, Sun Y X, et al. *Inorg. Chem. Commu.*, **2009**,**12**:234-236
[55]Zheng S S, Dong W K, Zhang Y, et al. *New J. Chem.*, **2017**, **41**:4966-4973
[56]Dong W K, Lan P F, Zhou W M, et al. *J. Coord. Chem.*,

2016,**69**:1272-1283

[57]Wang L, Dong X Y, Zhao L, et al. *Asian J. Chem.*, **2013**,**6**: 3440-3442

[58]Sheldrick G M. *Acta Crystallogr. Sect. A*: *Found. Crystallogr.*, **2008**,**A64**:112-122

[59]WANG Li(王莉), KANG Quan-Peng(康全鹏), HAO Jing(郝静), et al. *Chinese J. Inorg. Chem.*(无机化学学报), **2018**, **34**:525-533

[60]Dong X Y, Gao L, Wang F, et al. *Crystals*, **2017**,**7**:267

[61]Dong W K, Ma J C, Dong Y J, et al. *Polyhedron*, **2016**,**115**: 228-235

[62]Gao L, Wang F, Zhao Q, et al. *Polyhedron*, **2018**,**139**:7-16

[63]Ghosh K, Harms K, Chattopadhyay S. *Polyhedron*, **2017**, **123**:162-175

[64]Wang F, Liu L Z, Gao L, et al. *Spectrochim. Acta Part A*, **2018**,**203**:56-64

[65]Kang Q P, Li X Y, Zhao Q, et al. *Appl. Organomet. Chem.*, **2018**,**32**:e4379